Systems/Circuits

Estrous Cycle Plasticity in the Hyperpolarization-Activated Current I_h Is Mediated by Circulating 17β-Estradiol in Preoptic Area Kisspeptin Neurons

Richard Piet,[1] Ulrich Boehm,[2] and Allan E. Herbison[1]

[1]Centre for Neuroendocrinology and Department of Physiology, University of Otago, Dunedin 9054, New Zealand, and [2]Department of Pharmacology and Toxicology, University of Saarland School of Medicine, D-66421 Homburg, Germany

Circulating gonadal steroid hormones are thought to modulate a wide range of brain functions. However, the effects of steroid fluctuations through the ovarian cycle on the intrinsic properties of neurons are not well understood. We examined here whether gonadal steroids modulated the excitability of kisspeptin neurons located in the rostral periventricular region of the third ventricle (RP3V) of female mice. These cells are strongly implicated in sensing the high levels of circulating estradiol on proestrus to activate gonadotropin-releasing hormone (GnRH) neurons that, in turn, trigger ovulation. Electrophysiological studies were undertaken in brain slices from ovariectomized (OVX), diestrous, and proestrous kisspeptin-GFP mice. RP3V kisspeptin neurons exhibited marked changes in the hyperpolarization-evoked depolarizing sag and rebound firing across these groups. The hyperpolarization-activated current I_h was identified to be responsible for the depolarizing sag and was increased across OVX → diestrous → proestrous mice. Experiments in OVX mice given estradiol replacement identified an estradiol-dependent increase in I_h within RP3V kisspeptin neurons. I_h in these cells was found to contribute to their subthreshold membrane properties and the dynamics of rebound firing following hyperpolarizing stimuli in an estrous cycle-dependent manner. Only a minor role was found for I_h in modulating the spontaneous burst firing of RP3V kisspeptin neurons. These observations identify I_h as an ionic current that is regulated in a cyclical manner by circulating estradiol within the female brain, and suggest that such plasticity in the intrinsic properties of RP3V kisspeptin neurons may contribute to the generation of the preovulatory GnRH surge.

Introduction

The gonadal steroid estradiol (E_2) is known to regulate brain function and behavior by modulating neural plasticity (Brinton, 2009; Foy et al., 2010; Luine and Frankfurt, 2012; McEwen et al., 2012; Srivastava, 2012). While synaptic plasticity and network excitability have been demonstrated to fluctuate through the estrous cycle (Woolley and McEwen, 1992; Warren et al., 1995; Good et al., 1999; Bi et al., 2001; Scharfman et al., 2003), it remains unclear whether the intrinsic properties of individual neurons are modulated in a similar manner. As changes in intrinsic properties will alter information processing, determining the impact of estradiol on ion channels is important for understanding the modulation of brain function associated with physiological and age-related fluctuations in circulating estradiol.

Received March 7, 2013; revised May 16, 2013; accepted May 20, 2013.

Author contributions: R.P. and A.E.H. designed research; R.P. performed research; U.B. contributed unpublished reagents/analytic tools; R.P. and A.E.H. analyzed data; R.P. and A.E.H. wrote the paper.

This research was supported by the Health Research Council of New Zealand (R.P. and A.E.H.) and the Deutsche Forschungsgemeinschaft (U.B.). We thank Rob Porteous for technical assistance; and Dr. Karl Iremonger, Dr. Xinhuai Liu, and Simon de Croft for comments and suggestions.

The authors declare no competing financial interests.

Correspondence should be addressed to Allan E. Herbison, Centre for Neuroendocrinology, Department of Physiology, University of Otago School of Medical Sciences, P.O. Box 913, Dunedin 9054, New Zealand. E-mail: allan.herbison@otago.ac.nz.

DOI:10.1523/JNEUROSCI.1021-13.2013

 0270-6474/13/3310828-12$15.00/0

The neural network controlling the activity of gonadotropin-releasing hormone (GnRH) neurons is a valuable model for studying estradiol actions within the brain as endogenous fluctuations in circulating estradiol levels across the female estrous cycle engender marked functional plasticity upon these cells (Herbison, 2006). Curiously, estradiol has both negative and positive feedback actions within the network that act to suppress or enhance GnRH neuron activity, respectively. It is now well established in rodent models that the positive feedback actions of estradiol occur through estrogen receptor (ER) α-expressing primary afferents to GnRH neurons that have their cell bodies located in the rostral periventricular region of the third ventricle (RP3V) (Wintermantel et al., 2006; Glidewell-Kenney et al., 2007; Herbison, 2008). Recent evidence indicates that estradiol activates ERα-expressing kisspeptin neurons in the RP3V to transsynaptically stimulate GnRH neurons at the time of positive feedback (Smith et al., 2006; Adachi et al., 2007; Clarkson et al., 2008; Clarkson and Herbison, 2009; Liu et al., 2011). While it is clear that estradiol drives cyclical changes in RP3V *Kiss1* mRNA expression across the rodent estrous cycle (Smith et al., 2005, 2006), how this steroid may regulate the electrical excitability of these neurons is unknown.

To address this key issue, we examined a range of intrinsic and extrinsic properties of RP3V kisspeptin neurons using patch-clamp electrophysiology in acute brain slices from ovariectomized (OVX; low estradiol concentrations), diestrous

(intermediate estradiol), and proestrous (high estradiol) kisspeptin-GFP mice (Mayer et al., 2010). This revealed that the depolarizing sag—a hallmark of the hyperpolarization-activated current I_h—in RP3V kisspeptin neurons was markedly different in the three animal groups. We confirm that RP3V kisspeptin neurons express I_h and show that this current is upregulated in a cyclical manner in intact female mice by circulating estradiol. Finally, we provide evidence that the functional impact of I_h on the physiology of RP3V kisspeptin neurons varies during the estrous cycle. These observations point to a possible mechanism by which circulating estradiol may promote plasticity in the neural network responsible for the preovulatory GnRH surge.

Materials and Methods

Animals, surgery, and brain slice preparation

Adult female 2–4-month-old kisspeptin-IRES-Cre $^{+/-}$/ROSA26-CAGS-τGFP $^{+/-}$ (Kiss-GFP) mice on a mixed 129/SvJ, C57BL/6 background (Mayer et al., 2010) were group housed under conditions of controlled temperature (22 ± 2°C) and lighting (12 h light/dark cycles, with lights on at 7:00 A.M.) with *ad libitum* access to food and water. All mice used in this study were bred from homozygous kisspeptin-IRES-Cre mice crossed with homozygous Cre-dependent GFP (ROSA26-CAGS-τGFP) mice. The University of Otago Animal Ethics Committee approved all animal experimental protocols.

Estrous cycle stage was determined by daily vaginal smear each morning (Caligioni, 2009) and mice exhibiting at least two regular 4 or 5 d estrous cycles used on diestrus (appearance of leukocytes) or proestrus (nucleated epithelial cells). In some experiments, mice were bilaterally OVX under anesthesia and used 2 weeks later. In surge protocol experiments, mice were treated as reported previously (Wintermantel et al., 2006; Clarkson et al., 2008). Briefly, adult female Kiss-GFP mice were bilaterally OVX under anesthesia, and given subcutaneous SILASTIC implants containing 17-β-estradiol (1 μg/20 g body weight) according to Bronson (1981). Implants were made of 17-β-estradiol dissolved in ethanol and mixed with medical grade adhesive (0.1 mg/ml adhesive), which was then injected into 1-mm-internal-diameter SILASTIC tubing. Six days later, one group of mice was killed and used for electrophysiology (OVX+E), while the other group received a subcutaneous injection of estradiol benzoate (1 μg/20 g body weight) at 9:00 A.M. and was used for electrophysiology the following day (OVX+E+E).

Mice were killed by cervical dislocation and decapitated between 10:00 A.M. and 12:00 P.M. In our colony, the preovulatory luteinizing hormone surge commences between 3:30 and 5:30 P.M. on proestrus (de Croft et al., 2012). Coronal brain slices (200 μm thick) including the RP3V were cut with a vibratome (VT1000S; Leica) in an ice-cold solution containing the following (in mM): NaCl 87, KCl 2.5, $NaHCO_3$ 25, NaH_2PO_4 1.25, $CaCl_2$ 0.5, $MgCl_2$ 6, glucose 25, and sucrose 75. Slices were then incubated at 30°C for at least 1 h in artificial CSF (aCSF) containing the following (in mM): NaCl 120, KCl 3, $NaHCO_3$ 26, NaH_2PO_4 1, $CaCl_2$ 2.5, $MgCl_2$ 1.2, and glucose 10. All solutions were equilibrated with 95% O_2/5% CO_2.

Patch-clamp recordings

Slices were placed under an upright microscope fitted for epifluorescence (Olympus) and constantly perfused (1.5–2.0 ml/min) with warm (30–32°C) aCSF. RP3V GFP-expressing neurons located ≤80 μm lateral to the wall of the third ventricle, where GFP faithfully reports kisspeptin expression (de Croft et al., 2012), were targeted for electrophysiological recordings. GFP-expressing neurons were first visualized by brief fluorescence illumination, and subsequently were approached using infrared differential interference contrast optics.

Spontaneous firing was recorded using the minimally invasive cell-attached loose patch configuration. Recording electrodes (4–6 MΩ) pulled from borosilicate capillaries (Warner Instruments) with a horizontal puller (Sutter Instruments) were filled with aCSF including 10 mM HEPES. Low-resistance seals (10–30 MΩ) were achieved by applying either no suction or the lowest amount of suction required to detect spontaneous spikes. No additional negative pressure was subsequently applied during the course of a recording. Spontaneous spikes were recorded in the voltage-clamp mode.

Whole-cell recordings were performed in the presence of 10 μM CNQX and 5 μM gabazine to block AMPA and $GABA_A$ receptors, respectively, unless otherwise stated. In some experiments (see Figs. 3, 4, 5), voltage-gated sodium channels and T-type calcium channels were also inhibited by the addition of 0.5 μM TTX and 100–200 μM $NiCl_2$, respectively. Recording electrodes (3–4.5 MΩ) were filled with a solution containing the following (in mM): 140 K gluconate, 8 NaCl, 10 HEPES, 0.4 Na_2-GTP, 4 Mg-ATP, adjusted to pH 7.2 with KOH. The junction potential (≈15 mV) was not corrected for. $GABA_A$ receptor-mediated postsynaptic currents (IPSCs) were recorded with a high-chloride internal solution aimed at optimizing their detection (in mM): 130 KCl, 10 HEPES, 0.2 Na_2GTP, 2 MgATP, adjusted to pH 7.3 with KOH. The junction potential (≈4 mV) was not corrected for.

All electrophysiological signals were recorded using a Multiclamp 700B amplifier (Molecular Devices) connected to a Digidata 1440A digitizer (Molecular Devices). Signals were low-pass filtered at 2–4 kHz before being digitized at a rate of 10 kHz and stored on a personal computer. Series resistance was <25 MΩ, and recordings were discarded if a >20% change in this value occurred in the course of an experiment.

Data acquisition and analysis

Acquisition and all subsequent analysis were performed with pClamp 10 (Molecular Devices), MiniAnalysis 6 (Synaptosoft), and GraphPad Prism 5.

Whole-cell voltage-clamp. Basic membrane properties were determined in voltage-clamp within 1–2 min after establishing the whole-cell configuration. The input resistance, membrane time constant (tau), and membrane capacitance were acquired using the seal test function of the pClamp 10 clampex program.

Spontaneous AMPA receptor-mediated postsynaptic currents (EPSCs; recorded at −60 mV) and $GABA_A$ receptor-mediated PSCs (IPSCs; recorded at −70 mV) were collected >10 min after breaking in. PSC amplitude and kinetics were determined by averaging >100 events in individual cells. EPSC decays were fitted with monoexponential functions (10–90% range). IPSC decays were fitted with dual exponential functions, and the weighted decay was calculated as follows: $\text{decay}_{\text{weighted}} = ((\text{decay}_{\text{fast}} \times \text{amplitude}_{\text{fast}}) + (\text{decay}_{\text{slow}} \times \text{amplitude}_{\text{slow}}))/(\text{amplitude}_{\text{fast}} + \text{amplitude}_{\text{slow}})$.

Tail currents were evoked by hyperpolarizing the membrane from a holding potential of −50 to −120 mV for 1 s in 10 mV decrements before stepping back to a test potential of −60 mV. This value was chosen to minimize low-threshold activation of calcium channels, which were not always completely blocked by $NiCl_2$ at more positive test potentials (data not shown). Tail currents in individual neurons were considered present if their amplitude was greater than 2 SDs of the baseline current at −60 mV. Peak tail current amplitudes were measured and normalized to the membrane capacitance in each recorded neuron. The resulting current densities were plotted in activation curves as a function of the step potential. Normalized activation curves were well fitted by a Boltzmann sigmoid function, and the half-activation potential (V_{50}) and slope values were statistically compared in diestrous and proestrous mice using the extra sum-of-squares *F* test. Rise times of I_h were obtained by fitting the activation phase of the hyperpolarization-activated current (−120 mV step) using a monoexponential function.

Whole-cell current-clamp. The resting membrane potential was determined within 1–2 min after establishing the whole-cell configuration, in the current-clamp mode without injecting any current. The membrane potential of neurons was subsequently maintained around −60 mV by direct current injection, unless otherwise noted. The excitability of neurons was assessed by injecting depolarizing and hyperpolarizing currents (1 s steps, 5 pA increments). The rheobase was defined as the minimal step current amplitude that could evoke the firing of action potentials (APs). AP amplitude was quantified by measuring the overshoot of the first action potential evoked at rheobase. AP half-duration was measured as the duration of the waveform of that AP at its half-amplitude. Depolarizing sags and rebounds were measured in response to hyperpolarizing current steps adjusted in individual neurons (−20 to −100 pA) to reach

Table 1. Basic electrophysiological properties of RP3V kisspeptin neurons

	Resting membrane potential (mV)[a]	Input resistance (GΩ)[b]	Membrane time constant (ms)[c]	Membrane capacitance (pF)[d]	AP overshoot (mV)[e]	AP half-duration (ms)[f]	Rheobase (pA)[g]
OVX ($n = 21$ neurons, 6 mice)	−44.57 ± 1.12	1.49 ± 0.08	0.28 ± 0.02	16.75 ± 0.81	24.68 ± 1.19	0.91 ± 0.03	8.33 ± 0.80
Diestrus ($n = 21$ neurons, 5 mice)	−47.95 ± 1.82	1.25 ± 0.09†	0.36 ± 0.04	22.58 ± 1.48**	26.91 ± 1.91	0.82 ± 0.02*	8.81 ± 0.84
Proestrus ($n = 19$ neurons, 5 mice)	−46.39 ± 1.06	0.92 ± 0.08‡	0.26 ± 0.02	19.40 ± 0.92	21.61 ± 1.76	0.78 ± 0.02**	9.47 ± 1.20

Statistical comparisons were performed using one-way ANOVA and Newman–Keuls post-tests.

[a] $p = 0.23$.

[b] $F_{(2,58)} = 11.47$, $p = 0.0001$; †$p < 0.05$, OVX versus diestrus, and $p < 0.01$, diestrus versus proestrus; ‡$p < 0.001$, OVX versus proestrus.

[c] $F_{(2,57)} = 3.244$, $p = 0.046$, post-tests not significant.

[d] $F_{(2,57)} = 7.084$, $p = 0.002$; **$p < 0.01$, OVX versus diestrus.

[e] $p = 0.09$.

[f] $F_{(2,58)} = 6.456$, $p = 0.003$; *$p < 0.05$, OVX versus diestrus; **$p < 0.01$, OVX versus proestrus.

[g] $p = 0.70$.

an approximately −95 mV peak hyperpolarization. Depolarizing sags were quantified as the difference between peak and steady-state hyperpolarization, normalized to the peak hyperpolarization, and expressed as a percentage. Rebounds were quantified as the difference between the peak depolarization following the current injection and the membrane potential ≈1 s later. Membrane time constants were obtained by fitting from baseline to peak the rising phase of the membrane response to the hyperpolarizing current injection with a monoexponential function. Changes in membrane time constant were examined for equivalent values of peak hyperpolarization achieved by varying the amplitude of the input current before and during 4-ethylphenylamino-1,2-dimethyl-6-methylaminopyrimidinium chloride (ZD7288) application. Similar results were obtained when the current step amplitude was kept constant (data not shown).

Rebound firing was evoked by injecting hyperpolarizing step currents (0.5 s, 10 pA intervals). The membrane potential in control conditions was adjusted in individual recordings by direct current injection to optimize rebound firing of APs. The latency of the first rebound AP was calculated as the time between the end of the current injection and the peak of the first AP. Changes in latency were examined for equivalent values of steady-state hyperpolarization. Recordings were started >5 min after establishing the whole-cell configuration. The effects of ZD7288 in whole-cell recordings were examined >5 min after the beginning of the bath application. We found that this period is sufficient to inhibit the depolarizing sag (data not shown).

Loose patch. Spontaneous spikes were detected using the threshold-crossing method. Spike time-stamps were organized in 20 s bins in rate–meter graphs. Average firing rates were compared over 3 min periods immediately before and at the end of the 10 min bath application of ZD7288. In agreement with our previous findings (de Croft et al., 2012), ≈90% of RP3V kisspeptin neurons were spontaneously active. Only these neurons were included in the analysis. Recordings were categorized according to their firing patterns. The Poisson surprise method was used to detect bursts in trains of spikes, and a neuron was categorized as bursting if >50% of its spikes occurred in bursts, as reported previously (Ducret et al., 2010; de Croft et al., 2012). All other firing patterns were considered nonbursting.

Statistics. Values given in the text and illustrated in figures are mean ± SEM. Traces in Figures 3, 4, and 5 are averages of 3–10 sweeps. Traces in other figures are single sweeps. Statistical comparison was performed using Fisher's exact test, paired and unpaired *t* tests, or one-way and two-way ANOVA tests as appropriate (see text). The sample size used in statistical tests was the number of neurons. All experiments were replicated in at least three different mice in each group (unless otherwise stated in the text), and one to three slices were used from each mouse. Differences were considered significant for *p* values <0.05.

Drugs

CNQX, 6-imino-3-(4-methoxyphenyl)-1(6H)-pyridazinebutanoic acid hydrobromide (gabazine), and ZD7288 were purchased from Tocris Bioscience. TTX citrate was purchased from Alomone Labs. Other chemicals were purchased from Sigma and Thermo Fisher Scientific. CNQX (sodium salt), gabazine, TTX, and ZD7288 were dissolved in water to a stock concentration, kept at −20°C until use, and diluted to the appropriate concentration in aCSF. Drugs were delivered by bath application.

Results

We performed whole-cell patch-clamp recordings of RP3V kisspeptin neurons in slices obtained from OVX, diestrous, and proestrous Kiss-GFP female mice. GFP expression in RP3V kisspeptin neurons is independent of the ovarian steroid hormonal milieu in these mice, with >90% of GFP-expressing neurons synthesizing kisspeptin in the RP3V of female mice (de Croft et al., 2012), enabling us to record from genuine RP3V kisspeptin neurons throughout the estrous cycle and in OVX mice.

Electrophysiological properties of RP3V kisspeptin neurons

We first examined several intrinsic and extrinsic electrophysiological characteristics of RP3V kisspeptin neurons. The resting membrane potential and membrane time constant of RP3V kisspeptin neurons were not significantly different between any of the three groups (Table 1). However, input resistance was significantly different among all three groups, being highest in OVX mice, intermediate in diestrous mice, and lowest in proestrous mice (Table 1). In addition, membrane capacitance was found to be significantly higher only in diestrous mice compared with OVX animals (Table 1). In current-clamp, RP3V kisspeptin neurons fired action potentials in response to depolarizing current injections (1 s duration; Fig. 1*A*). While the rheobase and action potential amplitude were similar in RP3V kisspeptin neurons from OVX, diestrous, and proestrous mice, the action potential half-duration was significantly lower in intact mice compared with OVX animals (Table 1). No significant differences were found in the input–output curves of RP3V kisspeptin neurons in the three groups of mice (OVX: $n = 22$ neurons, 6 mice; diestrus: $n = 21$ neurons, 5 mice; proestrus: $n = 19$ neurons, 5 mice; two-way ANOVA, interaction $p = 0.66$; mouse group $p = 0.40$; Fig. 1*B*).

We also examined spontaneous synaptic currents in RP3V kisspeptin neurons. These neurons exhibited spontaneous EPSCs (recorded in the presence of 5 μM gabazine) and IPSCs (recorded in the presence of 10 μM CNQX) that were blocked completely by the AMPA receptor antagonist CNQX ($n = 4$ neurons, 3 diestrous mice; Fig. 2*A*) and by the $GABA_A$ receptor antagonist gabazine ($n = 5$ neurons, 2 diestrous mice; Fig. 2*C*), respectively. We found no significant differences in sEPSC (Fig. 2*B*) or sIPSC (Fig. 2*D*) amplitude (one-way ANOVA $p = 0.73$ and 0.62, respec-

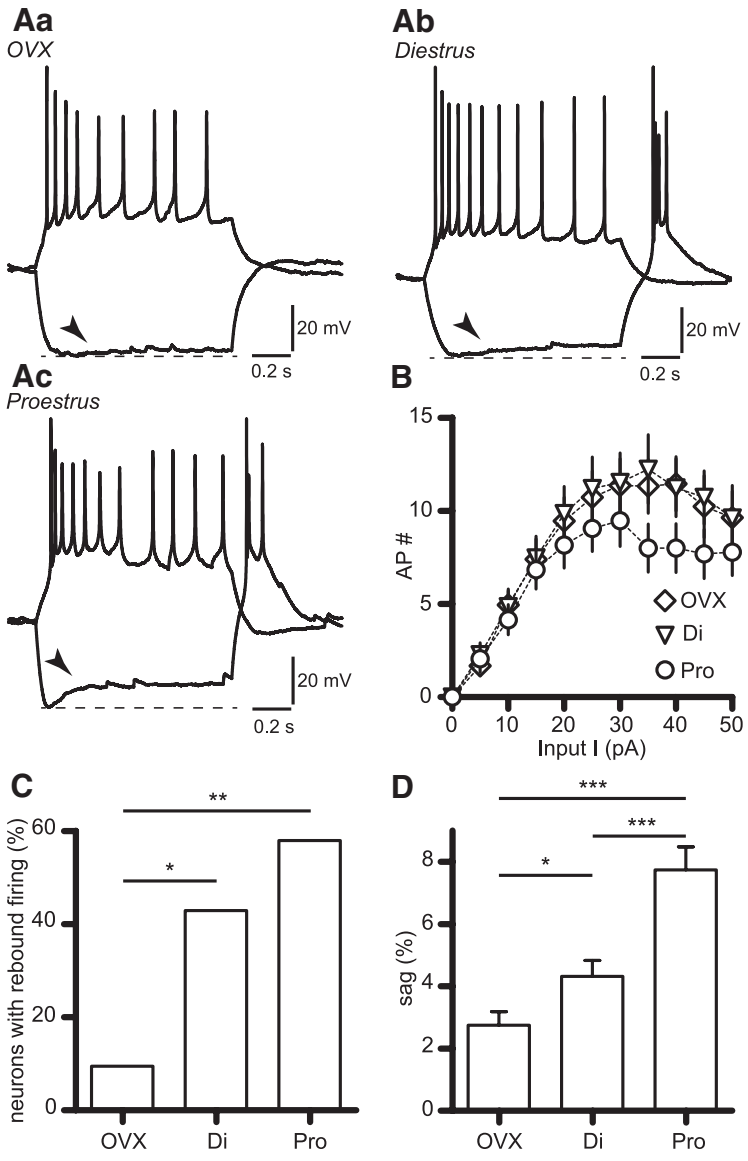

Figure 1. Depolarizing sag amplitude varies with gonadal status in RP3V kisspeptin neurons. ***A***, Example membrane responses of OVX (***Aa***), diestrous (***Ab***), and proestrous (***Ac***) RP3V kisspeptin neurons to hyperpolarizing (OVX: −40 pA; diestrus: −20 pA; proestrus: −50 pA) and depolarizing (OVX: 20 pA; diestrus: 10 pA; proestrus: 15 pA) current injections (1 s duration). Arrowheads indicate the depolarizing sag. ***B***, Input–output curves of AP firing evoked by depolarizing current injections in RP3V kisspeptin neurons from OVX ($n = 22$ neurons, 6 mice), diestrous (Di; $n = 21$ neurons, 5 mice), and proestrous mice (Pro; $n = 19$ neurons, 5 mice). ***C***, Proportion of RP3V kisspeptin neurons in each mouse group exhibiting rebound firing following hyperpolarization. ***D***, Histograms summarizing the amplitude of the depolarizing sag in OVX ($n = 21$ neurons, 6 mice), diestrus ($n = 21$ neurons, 5 mice), and proestrus ($n = 19$ neurons, 5 mice). *$p < 0.05$, **$p < 0.01$, ***$p < 0.001$.

tively), frequency ($p = 0.67$ and 0.24, respectively), or kinetics (rise time $p = 0.27$ and 0.11, respectively; decay $p = 0.45$ and 0.38, respectively) among OVX, diestrous, and proestrous mice.

RP3V kisspeptin neurons display a depolarizing sag

Upon hyperpolarization, RP3V kisspeptin neurons from intact mice displayed prominent depolarizing sags often followed by rebound firing of APs (Fig. 1*Ab*,*Ac*). Marked differences existed in the amplitude of the depolarizing sag and the prevalence of rebound firing across the different mouse groups. Only 2 of 21 (10%) RP3V kisspeptin neurons displayed rebound firing in OVX mice, compared with 9 of 21 (43%) in diestrus and 11 of 19 (58%) in proestrus ($p = 0.033$ and $p = 0.002$ vs OVX, respectively, Fisher's exact test; Fig. 1*C*). Furthermore, we found that the sag amplitude was lower in RP3V kisspeptin neurons from OVX mice (2.75 ± 0.44%, $n = 21$ neurons, 6 mice) than in those from intact mice. More importantly, the sag amplitude was larger in proestrous (7.74 ± 0.73%, $n = 19$ neurons, 5 mice, $p < 0.001$ vs OVX) than in diestrous RP3V kisspeptin neurons (4.33 ± 0.51%, $n = 21$ neurons, 5 mice, $p < 0.05$ and $p < 0.001$ vs OVX and proestrus, respectively; one-way ANOVA with Newman–Keuls post-test; $F_{(2,58)} = 20$, $p = 0.0001$; Fig. 1*D*). Of note, we also observed that RP3V kisspeptin neurons in intact mice exhibited a sag upon subthreshold depolarization. This hyperpolarizing sag, which results from deactivation of the channels mediating I_h (Biel et al., 2009), tended to be larger in proestrus (2.53 ± 0.77%, $n = 13$ neurons, 8 mice) than in diestrus (0.98 ± 0.38%, $n = 17$ neurons, 9 mice), although this was not significant ($p = 0.06$, unpaired t test; not illustrated).

Together, these results indicate that electrophysiological properties of RP3V kisspeptin neurons, and especially their responses to hyperpolarization, vary during the estrous cycle and are likely under the influence of gonadal steroids. As the hyperpolarization-activation inward current I_h underlies the depolarizing sag and contributes to rebound firing (Biel et al., 2009), we set out to study whether this current undergoes estrous cycle-dependent plasticity in RP3V kisspeptin neurons.

RP3V kisspeptin neurons express an I_h-like current

To isolate I_h and its functional effects, recordings were performed in the presence of 10 μM CNQX, 5 μM gabazine, 0.5 μM TTX, and 100–200 μM $NiCl_2$ to inhibit fast synaptic transmission, voltage-gated sodium channels, and low-threshold calcium channels, respectively.

In voltage-clamp, 1 s step hyperpolarizations from −50 to −120 mV (in 10 mV decrement) evoked tail currents of incrementing amplitude at a test potential of −60 mV in RP3V kisspeptin neurons from intact mice (Fig. 3*A*,*B*; diestrus and proestrus). We assessed the presence and magnitude of tail currents in kisspeptin neurons from OVX, diestrous, and proestrous mice. Tail currents were found in 6 of 15 (40%) OVX RP3V kisspeptin neurons (4 mice), whereas they could be readily detected in almost all neurons from intact mice (13 of 15 neurons in diestrus, 4 mice; 13 of 13 neurons in proestrus, 4 mice; $p = 0.021$ and $p = 0.0008$ OVX vs diestrus and proestrus, respectively; Fisher's exact test). Moreover, tail currents appeared larger in proestrous than in diestrous kisspeptin neurons (Fig. 3*A*). On average, activation curves revealed striking differences in the magnitude of tail current densities for step potentials less than or equal to −90 mV among the three groups of mice examined (Fig. 3*B*): tail current density

was lowest in OVX mice ($n = 15$ neurons, 4 mice), intermediate in diestrous mice ($n = 15$ neurons, 4 mice, $p < 0.05$ vs OVX), and largest in proestrous mice ($n = 13$ neurons, 4 mice, $p < 0.001$ vs OVX and diestrous mice, two-way ANOVA with Bonferroni post-test; interaction $F_{(14)} = 9.335$, $p = 0.0001$). Decreased mean current densities in OVX may be due to the lower proportion of RP3V kisspeptin neurons displaying tail currents as OVX tail current densities were not significantly different from those measured in diestrus when only neurons with detectable tail currents were considered (two-way ANOVA diestrus vs OVX; data not shown).

Normalized tail current activation curves were well fitted by a Boltzmann sigmoidal function (Fig. 3*C*), and both V_{50} (-76.2 ± 5.3 and -78.7 ± 3.0 mV) and slope (-9.1 ± 5.0 and -8.0 ± 2.8 mV) had similar values in diestrus and proestrus, respectively ($p = 0.91$, F test). We also examined the rise time of the hyperpolarization-activated current during steps to -120 mV. Rise times were well fitted by a monoexponential function in 9 and 10 recordings in diestrus and proestrus, respectively. The average time constants were of comparable value (diestrus 170.3 ± 33.7 ms; proestrus 135.1 ± 17.7 ms; $p = 0.35$, unpaired t test; not illustrated). These results suggest that hyperpolarization-activated currents in RP3V kisspeptin are mediated by similar ion channels in diestrous and in proestrous mice.

We next examined whether hyperpolarization-activated currents in RP3V kisspeptin neurons were sensitive to ZD7288, which inhibits I_h in neurons (Harris and Constanti, 1995). This experiment was performed in RP3V kisspeptin neurons from proestrous mice, where tail currents were prominent. As illustrated in Figure 3*D*, bath application of 10 μM ZD7288 completely abolished the tail currents, as well as the steady-state currents observed during the course of step hyperpolarization in all tested neurons. In addition, ZD7288 flattened the activation curve of the tail current, leaving virtually no residual tail current at any step potential ($n = 7$ neurons, 5 mice, interaction $F_{(7)} = 17.52$, $p = 0.0001$, two-way ANOVA with Bonferroni post-test; Fig. 3*E*). This finding indicates that most RP3V kisspeptin neurons in intact females express I_h and validates the use of our voltage-clamp protocol to detect and measure this current.

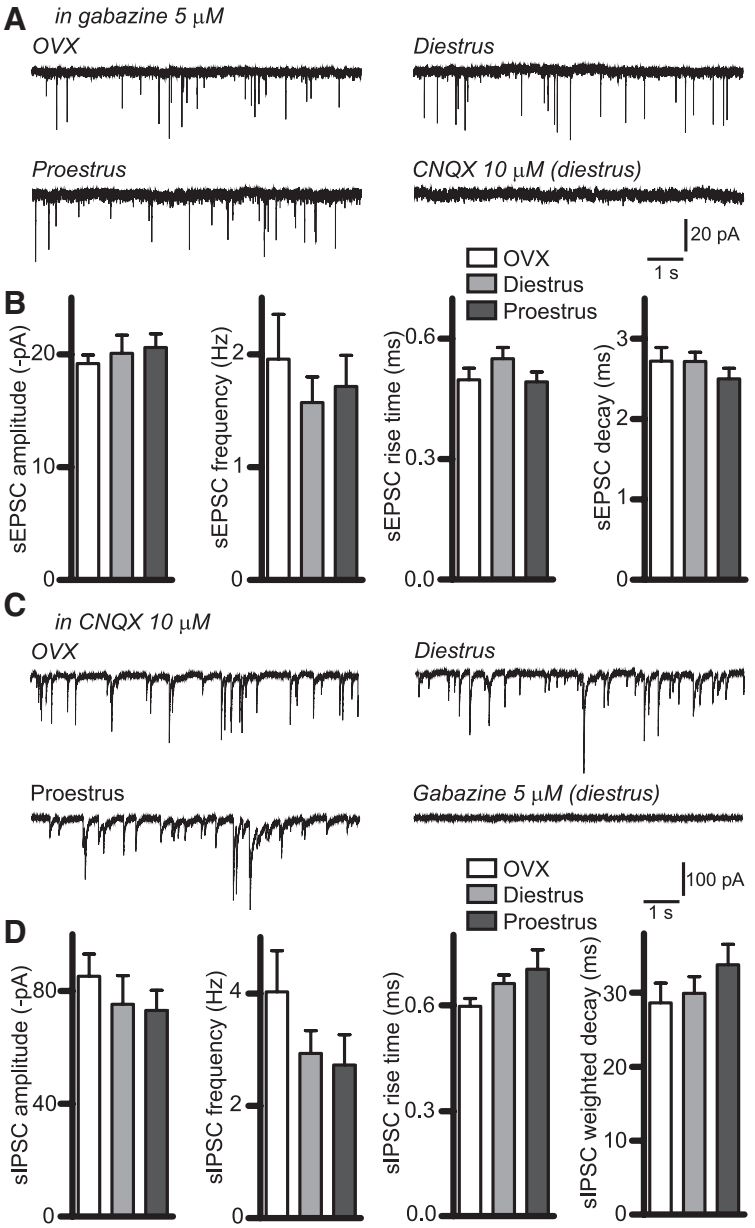

Figure 2. Spontaneous synaptic activity in RP3V kisspeptin neurons. ***A***, Sample traces illustrating sEPSCs recorded in OVX, diestrous, and proestrous RP3V kisspeptin neurons in the presence of 5 μM gabazine. Addition of 10 μM CNQX abolished sEPSCs. ***B***, Summary histograms of the amplitude, frequency, rise time, and decay of sEPSCs in the three mouse groups (OVX: $n = 18$ neurons, 6 mice; diestrus: $n = 19$ neurons, 7 mice; proestrus: $n = 19$ neurons, 6 mice). ***C***, Sample traces showing sIPSCs recorded in OVX, diestrous, and proestrous RP3V kisspeptin neurons in the presence of 10 μM CNQX; 5 μM gabazine abolished sIPSCs. ***D***, Summary histograms of the amplitude, frequency, rise time, and weighted decay of sIPSCs in the three mouse groups (OVX: $n = 18$ neurons, 4 mice; diestrus: $n = 22$ neurons, 5 mice; proestrus: $n = 15$ neurons, 4 mice).

I_h mediates the depolarizing sag and rebound in RP3V kisspeptin neurons

We next studied the membrane potential correlates of I_h in RP3V kisspeptin neurons recorded in current-clamp. As described above, kisspeptin neurons displayed a depolarizing sag upon hyperpolarization (1 s step current injection; Fig. 4*A*). Consistent with our findings on tail currents, the depolarizing sag magnitude, when studied in isolation, was lowest in OVX ($2.17 \pm 0.48\%$, $n = 15$ neurons, 4 mice), intermediate in diestrous ($4.25 \pm 0.56\%$, $n = 15$ neurons, 4 mice), and largest in proestrous kisspeptin neurons ($8.38 \pm 1.16\%$, $n = 13$ neurons, 4 mice; Fig. 4*B*; $p < 0.001$ compared with OVX and diestrus; $F_{(2,40)} = 16.86$, $p = 0.0001$, one-way ANOVA with Newman–Keuls post-test). No significant difference was detected between OVX and diestrus using one-way ANOVA, although this was significant when analyzed by unpaired t test ($t_{(28)} = 2.808$, $p = 0.009$). RP3V kisspep-

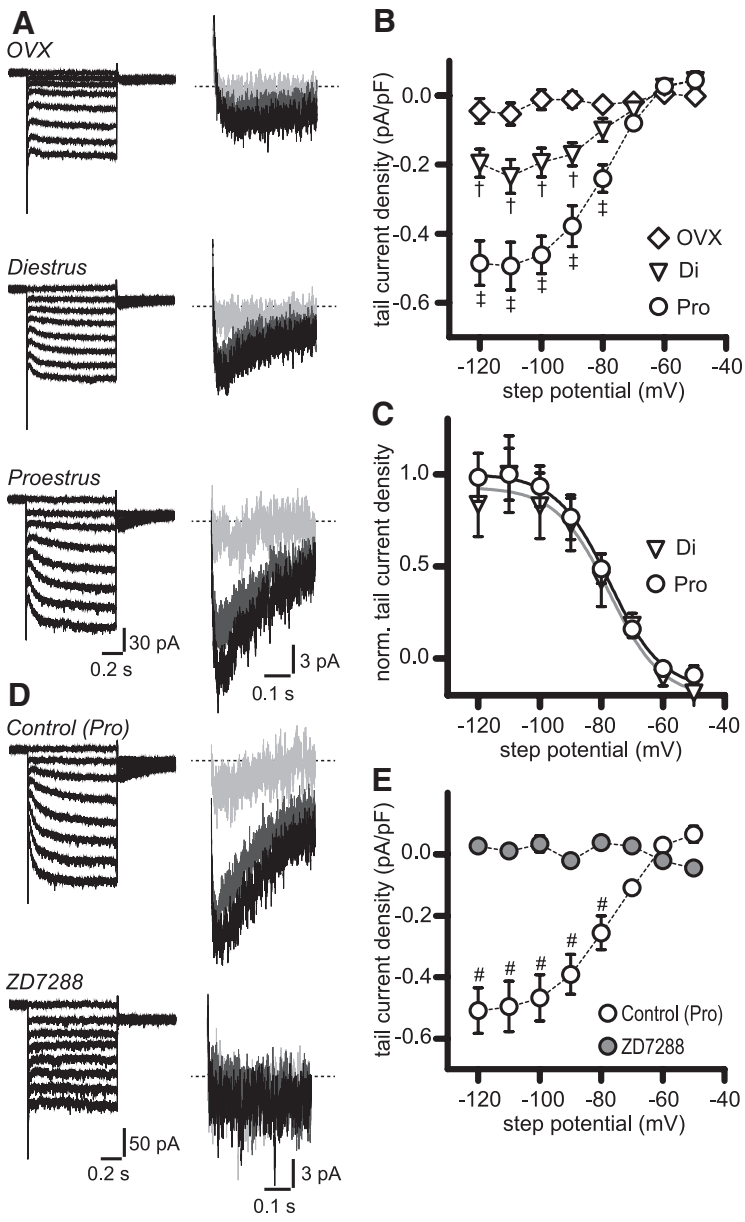

Figure 3. I_h-like currents in RP3V kisspeptin neurons are upregulated in proestrous mice. ***A***, membrane currents in response to voltage steps from −50 to −120 mV (left) in OVX, diestrous, and proestrous RP3V kisspeptin neurons in the presence of a cocktail of synaptic and ion channel blockers (see Results). Tail currents (expanded views, right) were apparent upon return to the test potential (−60 mV). Only tail currents corresponding to −70 (light gray), −90 (dark gray), and −110 mV steps (black) are illustrated for clarity. ***B***, Activation curves of tail currents in OVX ($n = 15$ neurons, 4 mice), diestrus (Di; $n = 15$ neurons, 4 mice), and proestrus (Pro; $n = 13$ neurons, 4 mice). Data points are connected by dotted lines. $^{\dagger}p < 0.05$ and $p < 0.001$ diestrus versus OVX and proestrus, respectively; $^{\ddagger}p < 0.001$ OVX versus proestrus; two-way ANOVA with Bonferroni post-test. ***C***, Normalized activation curves in diestrus and proestrus. Gray and black lines represent Boltzmann sigmoidal fits to diestrous and proestrous curves, respectively. ***D***, Example traces illustrating the blockade of hyperpolarization-activated steady-state and tail currents by 10 μM ZD7288 (bottom traces). ***E***, ZD7288 flattened the activation curve of hyperpolarization-activated tail currents ($n = 7$ neurons, 5 mice). $^{\#}p < 0.0001$ control versus ZD7288; two-way ANOVA with Bonferroni post-test.

tin neurons also displayed a rebound depolarization upon termination of the current injection (Fig. 4*A*). Similar to the depolarizing sag, the rebound was most prominent in proestrous neurons (5.62 ± 0.85 mV, $n = 13$ neurons, 4 mice) compared with diestrous (2.33 ± 0.40 mV, $n = 15$ neurons, 4 mice) and OVX kisspeptin neurons (0.50 ± 0.21 mV neurons, $n = 15$, 4 mice). In this case, all values were significantly different from one another ($p < 0.05$ and $p < 0.001$ OVX vs diestrus and proestrus, respectively; $p < 0.001$ diestrus vs proestrus; one-way ANOVA with Newman-–Keuls post-test; $F_{(2,40)} = 23.78$, $p = 0.0001$; Fig. 4*B*). As illustrated in Figure 4*C*, 10 μM ZD7288 inhibited the depolarizing sag and rebound in proestrous kisspeptin neurons by ≈90% (sag: 9.61 ± 1.09% to 0.95 ± 0.43%; rebound: 5.84 ± 1.01 to 0.68 ± 0.21 mV; $n = 6$ neurons, 4 mice; $t_{(5)} = 10.47$, $p = 0.0001$ and $t_{(5)} = 4.286$, $p = 0.0078$, respectively, paired t test, Figure 4*D*), showing that I_h underlies both events.

Together, these findings indicate the presence of an I_h-like current, and its associated depolarizing sag and rebound, in female RP3V kisspeptin neurons and that it is dependent on circulating ovarian steroids with maximal expression in proestrous neurons.

Circulating estradiol upregulates I_h in RP3V kisspeptin neurons

We next examined whether E_2 is involved in modulating I_h in RP3V kisspeptin neurons. To address this question, we used a well established mouse model in which OVX+E mice exhibit negative feedback similar to diestrous mice and OVX+E+E animals represent the high estrogen state of positive feedback observed on proestrus (Bronson and Vom Saal, 1979). In OVX+E mice, I_h as well as the depolarizing sag and rebound could be readily detected in most RP3V kisspeptin neurons (17 of 18, 3 mice; Fig. 5*A*,*C*) Importantly, RP3V kisspeptin neurons in OVX+E+E mice exhibited I_h tail current densities that were significantly larger (OVX+E: $n = 18$ neurons, 3 mice; OVX+E+E: $n = 17$ neurons, 3 mice; interaction: $F_{(7)} = 11.50$, $p = 0.0001$, two-way ANOVA with Bonferroni post-test; Fig. 5*B*). Normalized activation curve fits yielded similar V_{50} and slope values in OVX+E and OVX+E+E RP3V kisspeptin neurons (OVX+E: −72.6 ± 4.0 and −9.1 ± 3.5 mV, respectively; OVX+E+E: −69.1 ± 2.4 and −8.7 ± 1.9 mV, respectively; $p = 0.61$ F test). Similarly, rise times of I_h currents (−120 mV steps) were comparable in the two groups of mice (OVX+E: 131.20 ± 13.49 ms, $n = 16$ neurons, 3 mice; OVX+E+E: 107.50 ± 11.29 ms, $n = 17$ neurons, 3 mice; $p = 0.19$, unpaired t test).

As seen in Figure 5*C*, the depolarizing sag and rebound were also increased in OVX+E+E compared with OVX+E mice. On average, the depolarizing sag and the rebound were significantly larger in OVX+E+E (9.42 ± 0.57% and 6.57 ± 0.69 mV, respectively; $n = 17$ neurons, 3 mice) compared with OVX+E (5.20 ± 0.52% and 3.37 ± 0.38 mV, respectively; $n = 18$ neurons, 3 mice; $t_{(33)} = 5.447$, $p = 0.0001$, and $t_{(33)} = 4.151$, $p = 0.0002$, respectively, unpaired t test).

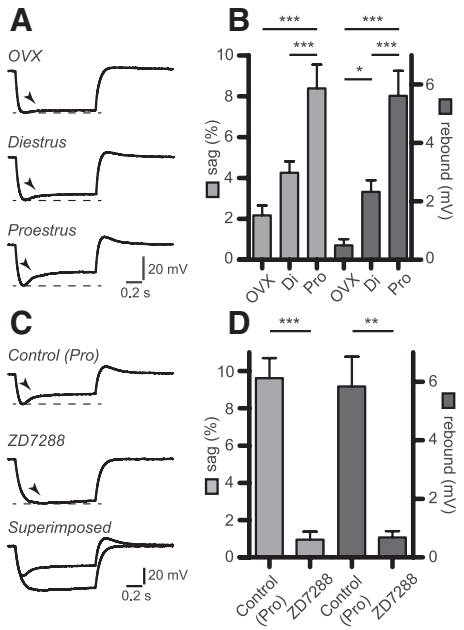

Figure 4. I_h-dependent depolarizing sag and rebound are upregulated in proestrous mice. ***A***, Example traces illustrating the depolarizing sag and rebound seen in OVX, diestrous, and proestrous RP3V kisspeptin neurons in response to hyperpolarizing current injections in the presence of a cocktail of synaptic and ion channel blockers (see Results). Arrowheads indicate the depolarizing sag. ***B***, Histograms summarizing the amplitude of the depolarizing sag and rebound in OVX ($n = 15$ neurons, 4 mice), diestrus (Di; $n = 15$ neurons, 4 mice), and proestrus (Pro; $n = 13$ neurons, 4 mice). ***C***, ***D***, In proestrous RP3V kisspeptin neurons, both sag and rebound were inhibited by 10 μM ZD7288 ($n = 6$ neurons, 4 mice). *$p < 0.05$, **$p < 0.01$, ***$p < 0.001$.

These observations reveal that increasing circulating E_2 is sufficient for upregulating I_h in RP3V kisspeptin neurons. This indicates that the increase in I_h observed in proestrous RP3V kisspeptin neurons results from the high E_2 concentrations found during the late follicular phase.

Blocking I_h does not alter spontaneous firing in RP3V kisspeptin neurons

To address the role of I_h in shaping the electrical activity of RP3V kisspeptin neurons, we performed on-cell loose patch recordings of the spontaneous firing of these neurons and tested the effect of blocking I_h with ZD7288. These experiments were performed in proestrous mice where I_h is prominent, and in the absence of synaptic blockers or of other ion channel inhibitors. As reported previously (Ducret et al., 2010; de Croft et al., 2012), RP3V kisspeptin neurons exhibited various patterns of spontaneous firing (Fig. 6*A*,*C*). Bath application of 10 μM ZD7288, a concentration that virtually abolishes I_h (see above), had no effect on the spontaneous firing of proestrous, nonbursting RP3V kisspeptin neurons (Fig. 6*B*; control: 2.77 ± 0.41 Hz; ZD7288: 2.78 ± 0.38 Hz; $n = 8$ neurons, 4 mice; $p = 0.89$, paired t test).

Because I_h is involved in the generation of bursts of action potentials in some neurons (Pape, 1996) and is hypothesized to play such a role in arcuate kisspeptin neurons (Gottsch et al., 2011), we further examined whether I_h played any role in the population of RP3V kisspeptin neurons that are spontaneously bursting. As illustrated in Figure 6*C*, blocking I_h did not prevent spontaneous bursting in these neurons, and on average, the mean firing rate of bursting neurons was not altered by ZD7288 (Fig. 6*D*; control: 1.17 ± 0.11 Hz; ZD7288: 1.17 ± 0.15 Hz; $n = 6$ neurons, 5 mice; $p = 0.99$, paired t test). Because the mean firing rate may not reflect potential changes in burst characteristics, we also quantified several parameters describing burst firing. ZD7288 was found to generate a significant ($t_{(5)} = 2.625$, $p = 0.047$, paired t test) increase in intraburst frequency, leaving the burst rate, the number of spikes/burst, the burst duration, and the proportion of spikes occurring in bursts unaffected (Table 2).

These results indicate that I_h does not contribute substantially to the spontaneous firing rate or pattern of RP3V kisspeptin neurons. In addition, these findings reveal that I_h plays only a minor role in the generation and/or modulation of burst firing in these neurons.

Effect of blocking I_h on basic membrane properties

The results described above indicate that I_h does not affect the electrical activity of RP3V kisspeptin neurons at rest. This is consistent with the activation curves of the tail current, which revealed little activation of this current at membrane potentials above −70 mV (Fig. 3*B*). We therefore examined the physiological consequences of I_h on the response of RP3V kisspeptin neurons to membrane hyperpolarization.

Current-clamp recordings were obtained from diestrous and proestrous RP3V kisspeptin neurons, and depolarizing sags were evoked by injecting 0.5-s-long hyperpolarizing step currents in the presence of 10 μM CNQX and 5 μM gabazine. The blockade of the depolarizing sag by 10 μM ZD7288 resulted in a significant increase in input resistance in diestrous (0.62 ± 0.05 to 0.88 ± 0.07 GΩ; $n = 11$ neurons, 4 mice; $t_{(10)} = 5.508$, $p = 0.0003$; paired t test; Fig. 7*A*) and proestrous RP3V kisspeptin neurons (0.62 ± 0.05 to 1.01 ± 0.09 GΩ; $n = 11$ neurons, 5 mice; $t_{(10)} = 7.090$, $p = 0.0001$; paired t test; Fig. 7*A*). Although it tended to be larger in proestrus, the fractional increase in input resistance was not significantly different in diestrus and in proestrus (45.93 ± 9.74% and 66.78 ± 8.91%, respectively, $p = 0.13$, unpaired t test; Fig. 7*B*).

We then measured membrane time constants in the presence and absence of 10 μM ZD7288 by fitting the rise time of the membrane potential response to the hyperpolarizing current injection (Fig. 7*A*). For comparable peak hyperpolarizations (≈−95 mV), τ values were significantly increased by ZD7288 in diestrous (25.47 ± 1.84 ms to 34.84 ± 2.48 ms; $n = 10$ neurons, 4 mice; $t_{(9)} = 4.929$, $p = 0.0008$, paired t test) as well as in proestrous RP3V kisspeptin neurons (30.77 ± 2.60 ms to 51.76 ± 6.16 ms; $n = 11$ neurons, 5 mice; $t_{(10)} = 4.602$, $p = 0.001$, paired t test). Importantly, the fractional ZD7288-induced increase in tau was larger in proestrous than in diestrous neurons (69.94 ± 11.66% and 39.14 ± 8.24%, respectively; $t_{(19)} = 2.117$, $p = 0.048$; unpaired t test; Fig. 7*C*). Similar results were obtained when the input hyperpolarizing current was kept constant, inducing larger peak hyperpolarizations in the presence of ZD7288 (approximately −110 mV; data not shown).

Thus, pharmacological blockade of I_h revealed that, consistent with its upregulation in proestrus, the contribution of this current to subthreshold membrane properties is larger in proestrous than in diestrous RP3V kisspeptin neurons.

I_h regulates the firing of rebound APs in RP3V kisspeptin neurons

RP3V kisspeptin neurons exhibiting prominent depolarizing sags also had large rebounds (for example, see Figs. 4*A*, 5*C*). In addition, as seen in Figure 1, the post-hyperpolarization rebound was associated with AP firing in ≈50% of RP3V kisspeptin neurons in diestrous and proestrous female mice but only in ≈10% in OVX mice, suggesting that I_h might be involved in rebound firing. We

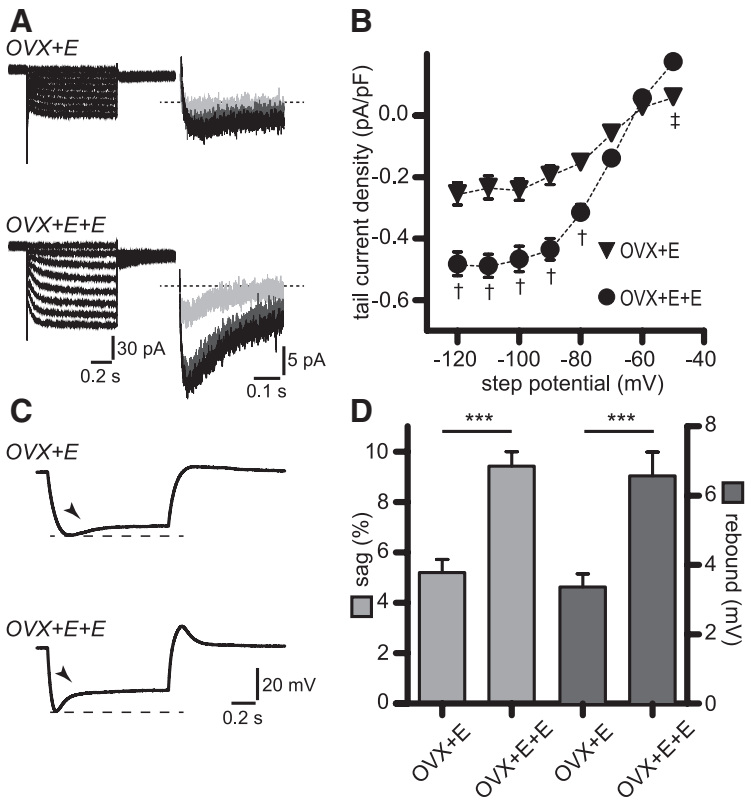

Figure 5. Upregulation of I_h and associated sag and rebound is mimicked by high circulating estradiol levels in a luteinizing hormone-surge protocol. ***A***, Membrane currents in OVX+E and OVX+E+E RP3V kisspeptin neurons in response to voltage steps from −50 to −120 mV in the presence of a cocktail of synaptic and ion channel blockers (see Results). Steady-state (left) and tail currents (right) were larger in OVX+E+E. Only tail currents corresponding to −70 (light gray), −90 (dark gray), and −110 mV steps (black) are illustrated for clarity. ***B***, Corresponding tail current activation curves illustrating the upregulation of I_h in OVX+E+E. OVX+E: $n = 18$ neurons, 3 mice; OVX+E+E: $n = 17$ neurons, 3 mice. $^{\dagger}p < 0.001$, $^{\ddagger}p < 0.05$ two-way ANOVA with Bonferroni post-test. ***C***, Example traces illustrating the depolarizing sag and rebound seen in OVX+E and OVX+E+E RP3V kisspeptin neurons in response to the hyperpolarizing current injections. Arrowheads indicate the depolarizing sag. ***D***, Histogram summarizing the sag and rebound amplitudes in OVX+E and OVX+E+E. OVX+E: $n = 18$ neurons, 3 mice; OVX+E+E: $n = 17$ neurons, 3 mice; $^{***}p < 0.001$.

therefore examined the contribution of I_h to the firing of rebound APs in diestrous and proestrous RP3V kisspeptin neurons. In these experiments, TTX and $NiCl_2$ were omitted.

Blocking I_h with 10 μM ZD7288 in the absence of $NiCl_2$ prevented rebound firing in only 1 of 10 diestrous and 2 of 11 proestrous RP3V kisspeptin neurons, indicating that although I_h provides rebound depolarization (Fig. 4), this current is not required for rebound firing in most RP3V kisspeptin neurons (Fig. 8*A*). However, blocking I_h did result in alterations in the timing of rebound firing (Fig. 8*A*). ZD7288 significantly increased the latency to the first rebound AP in diestrous kisspeptin neurons (103.2 ± 12.3 to 135.9 ± 17.8 ms; $n = 9$ neurons, 4 mice; $t_{(8)} = 4.171$, $p = 0.003$, paired t test). In proestrous kisspeptin neurons, latencies were not only doubled by ZD7288 (111.0 ± 15.0 to 226.8 ± 31.6 ms; $n = 9$ neurons, 5 mice; $t_{(8)} = 5.657$, $p = 0.0005$, paired t test), but the fractional ZD7288-induced increase in latency was significantly larger than in diestrus (108.5 ± 20.6 vs 31.5 ± 6.6%; $n = 9$ neurons, 5 mice and $n = 9$ neurons, 4 mice, respectively; $t_{(16)} = 3.553$, $p = 0.003$, unpaired t test; Fig. 8*B*). The number of APs fired on rebound was not significantly affected by ZD7288 in diestrus (control: 1.8 ± 0.2; ZD7288: 1.6 ± 0.2; $n = 9$ neurons, 4 mice; $p = 0.35$, paired t test) or in proestrus (control: 2.0 ± 0.3; ZD7288: 2.4 ± 0.4; $n = 9$ neurons, 5 mice; $p = 0.17$, paired t test; not illustrated).

This observation reveals that I_h plays a more important role in shaping rebound firing in proestrus than in diestrus, in agreement with the finding that I_h is more prominent in proestrous RP3V kisspeptin neurons.

Last, we sought to determine what triggers the firing of rebound APs in the absence of I_h. In proestrous RP3V kisspeptin neurons, we first applied ZD7288 to block I_h. In neurons that kept firing rebound APs (6 of 8), 200 μM $NiCl_2$, a low-threshold calcium channel inhibitor, abolished rebound firing (Fig. 7*C*; $n = 6$ neurons, 4 mice). This finding, along with the above data, indicates that low threshold calcium channels, possibly T-type channels, work in concert with channels mediating I_h in RP3V kisspeptin neurons, and presumably with other ion channels, to trigger and fine tune the firing of rebound APs.

Discussion

Estradiol regulation of RP3V kisspeptin neurons

There is substantial evidence indicating that estrogen stimulates RP3V kisspeptin neurons to activate GnRH neurons at the time of the preovulatory luteinizing hormone surge (Clarkson and Herbison, 2009; Oakley et al., 2009). How circulating estradiol impacts upon RP3V kisspeptin neuron excitability is unknown. By examining a variety of intrinsic and extrinsic properties of kisspeptin neurons in OVX, diestrous, and proestrous mice, we identify here that estradiol exerts a potent stimulatory influence upon I_h in these cells. In addition, we note that both the input resistance and action potential half-width of kisspeptin neurons is reduced across across OVX → diestrous → proestrous mice. Whereas the variation observed in input resistance is likely to be at least partly attributable to changes in I_h, the modulation of action potential width raises the possibility of an estrogen-regulated potassium channel in kisspeptin neurons. In terms of synaptic inputs to RP3V kisspeptin neurons, we find that spontaneous AMPA and $GABA_A$ receptor-mediated PSCs are not different in OVX, diestrous, and proestrous mice. A recent study reported that estradiol treatment of OVX mice altered IPSC amplitude in RP3V kisspeptin neurons (Frazão et al., 2013). A similar change was not detected here between OVX and intact mice, although we note that our use of a high intracellular chloride ion concentration has allowed us to detect a 10-fold higher frequency of sIPSCs in kisspeptin neurons compared with Frazão et al. (2013). Together, the present findings indicate that estradiol modulates specific ion channels underlying the intrinsic properties of RP3V kisspeptin neurons with changes in I_h being prominent.

Estradiol-dependent upregulation of I_h in RP3V kisspeptin neurons

The hyperpolarization-activated inward current in RP3V kisspeptin neurons observed in intact female mice activates slowly, shows little inactivation, and is inhibited by ZD7288, consistent

with known properties of I_h (Robinson and Siegelbaum, 2003; Biel et al., 2009). Similar I_h-like currents have been detected in the other main population of kisspeptin neurons, located in the arcuate nucleus, of female mice and guinea pigs (Gottsch et al., 2011; Qiu et al., 2011). I_h is mediated by a family of hyperpolarization and cyclic nucleotide (HCN) gated channels assembled in tetraheteromeres or tetrahomomeres and displaying various functional properties (Biel et al., 2009). Although HCN4 subunits can likely be ruled out in RP3V kisspeptin neurons due to their slow kinetics, identifying precisely which HCN subunits make up the channels mediating I_h in these cells cannot be determined from the present data.

Precisely how estradiol modulates I_h in RP3V kisspeptin neurons remains to be determined, but several possibilities can be envisioned. HCN channels are gated by hyperpolarization and by intracellular second messengers (DiFrancesco and Tortora, 1991; Santoro et al., 1998; Pian et al., 2006; Zolles et al., 2006). Such regulation typically involves shifts in the activation curve of I_h (Biel et al., 2009). Although we cannot rule out any involvement of this type of regulation, our observation that I_h activation curves are similar in RP3V kisspeptin neurons across the estrous cycle makes it an unlikely scenario. For the same reason, a change in HCN channel subunits in RP3V kisspeptin neurons seems unlikely. I_h current density could also be increased via alterations in the trafficking of HCN channels to the plasma membrane. HCN channels in the brain interact with TRIP8b (Santoro et al., 2004), a protein with splice variants that have multiple effects on HCN channel trafficking, targeting, and gating (Lewis et al., 2009; Piskorowski et al., 2011). Whether this is relevant to RP3V kisspeptin neurons remains to be determined. Interestingly, a study undertaken in gonadectomized male mice has reported that E_2 decreases I_h expression in GnRH neurons (Chu et al., 2010). The direction of E_2 regulation is opposite to what we have observed here in RP3V kisspeptin neurons and suggests that the regulation of I_h by gonadal steroids may be cell type and/or sex dependent.

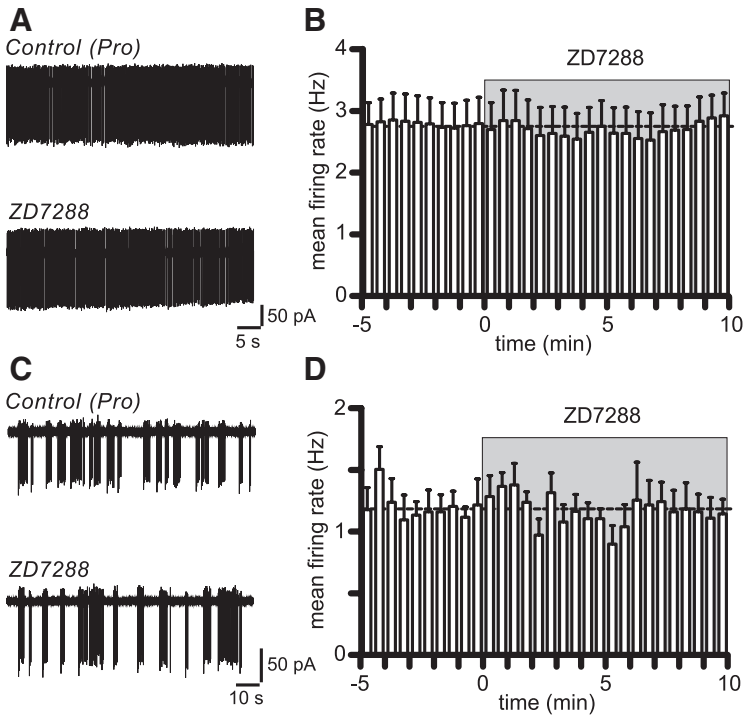

Figure 6. Blocking I_h does not alter the spontaneous firing of proestrous RP3V kisspeptin neurons. ***A***, Example traces illustrating the lack of effect of 10 μM ZD7288 in a nonbursting proestrous RP3V kisspeptin neuron. ***B***, Summary rate meter histogram of the mean firing rate of RP3V kisspeptin neurons. ZD7288 did not change the firing rate of nonbursting RP3V kisspeptin neurons (n = 8 neurons, 4 mice). ***C***, Traces illustrating the firing of a proestrous, bursting RP3V kisspeptin neuron in the absence and in the presence of ZD7288. ***D***, On average, bursting RP3V kisspeptin neurons did not change their firing rate in response to ZD7288 (n = 6 neurons, 5 mice).

Table 2. Burst parameters in proestrous RP3V kisspeptin neurons in the presence and in the absence of ZD7288 (n = 6 neurons, 5 mice)

	Burst rate (min^{-1})	Spikes/burst	Intraburst frequency (Hz)	Burst duration (s)	Spikes in bursts (%)
Control	5.44 ± 0.46	10.42 ± 0.62	3.42 ± 0.14	3.29 ± 0.24	82.8 ± 5.2
ZD288	5.66 ± 0.41	9.46 ± 0.88	3.81 ± 0.21	2.76 ± 0.24	78.4 ± 6.5
Paired t test	$p = 0.71$	$p = 0.26$	$p = 0.047$	$p = 0.15$	$p = 0.59$

Functional consequences

The physiological roles of I_h in the modulation of neural activity are multiple, including the control of membrane potential, pacemaker activity, and basic membrane properties (Robinson and Siegelbaum, 2003). In RP3V kisspeptin neurons, control of the membrane potential by I_h is evidenced by the depolarizing sag in response to hyperpolarization, showing that this current will counteract inhibition. This effect is more prominent in proestrous mice, where the depolarizing sag is larger, indicating that during that stage of the cycle RP3V kisspeptin neurons will be less sensitive to membrane hyperpolarization. We also found that RP3V kisspeptin neurons exhibited a hyperpolarizing sag upon subthreshold membrane depolarization and this displayed a nonsignificant trend to be larger in proestrus than in diestrus. This suggests that I_h may also act to stabilize the membrane potential in RP3V kisspeptin neurons, as it does in other cells (Biel et al., 2009).

We report that blocking I_h has little effect on the spontaneous firing of RP3V kisspeptin neurons, implying that I_h plays no significant role in controlling the firing of these neurons at rest in our recording conditions. Consistent with this, tail current activation curves reveal that half activation of I_h occurs between −75 and −80 mV, and that little I_h activity exists at potentials positive to −70 mV. I_h has been implicated in burst firing and pacemaking in thalamic neurons, where it is thought to provide the initial depolarization that eventually activates low threshold calcium channels and burst firing (Pape, 1996; McCormick and Bal, 1997). Here, we observe that spontaneously bursting RP3V kisspeptin neurons can still fire in bursts in the presence of ZD7288, indicating that I_h is not involved in these events. This suggests that burst firing seen in loose patch recordings of RP3V kisspeptin neurons (Ducret et al., 2010; de Croft et al., 2012) is the result of membrane events distinct to those responsible for burst firing in other neurons. The finding that blocking I_h does not alter spontaneous firing of RP3V kisspeptin neurons, be it bursting or nonbursting, reveals that I_h does not act as a pacemaker current in these neurons. Consistent with this, we reported previously that the spontaneous firing of these neurons is unchanged be-

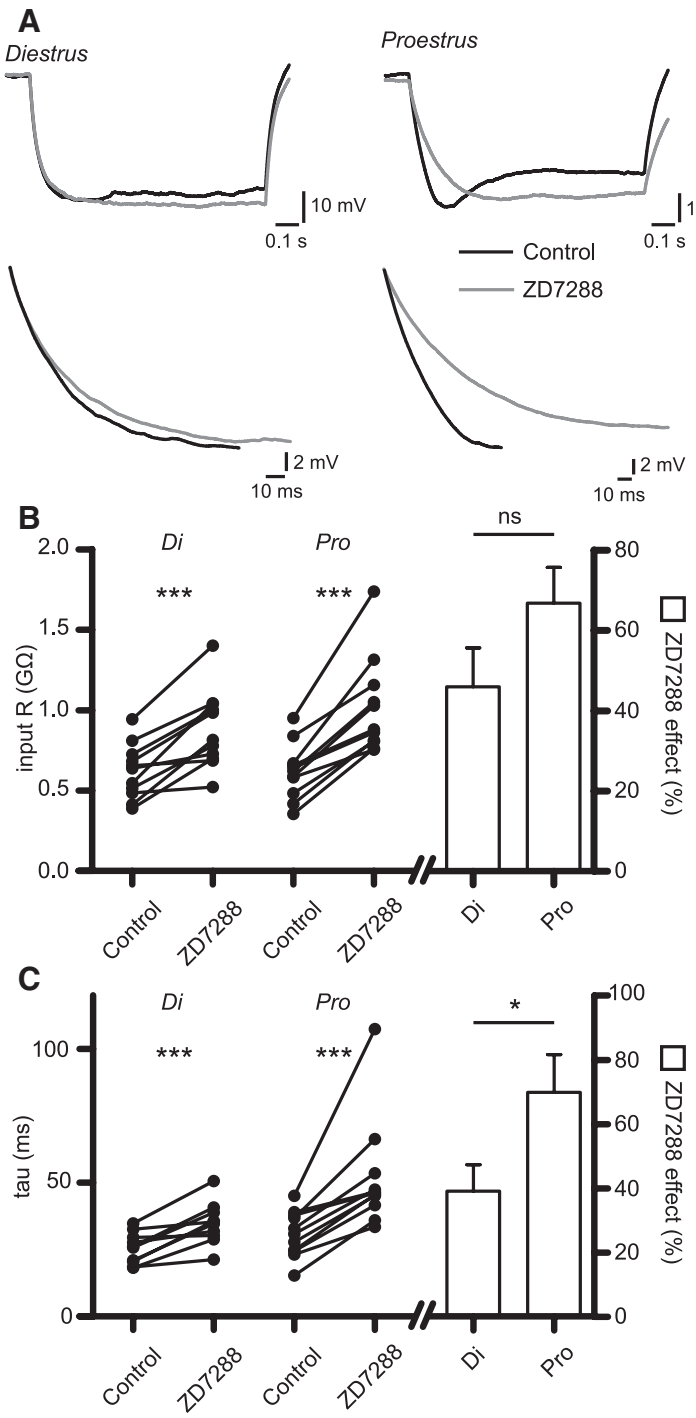

Figure 7. I_h differentially alters basic membrane properties in diestrous and proestrous RP3V kisspeptin neurons. ***A***, Membrane hyperpolarization in diestrous and proestrous RP3V kisspeptin neurons in response to a 0.5 s step current injection in the absence (black trace) and in the presence (gray trace) of 10 μM ZD7288. Current injection was adjusted in the proestrous neuron to account for the ZD7288 increase in input resistance and reach a similar peak hyperpolarization (control: −50 pA; ZD7288: −30 pA). The same traces at a higher time resolution are shown below, illustrating the larger ZD7288-induced slowing of the membrane time constant in proestrous RP3V kisspeptin neurons. ***B***, Summary graph of the effect of ZD7288 on input resistance in diestrous (n = 11 neurons, 4 mice) and proestrous (n = 11 neurons, 5 mice) kisspeptin neurons. ***C***, Summary graph of the effect of ZD7288 on the membrane time constant of RP3V kisspeptin neurons in diestrus (n = 10 neurons, 4 mice) and proestrus (n = 11 neurons, 5 mice). ns, Not significant, *$p < 0.05$, ***$p < 0.001$.

tween diestrous and proestrous mice in slices (de Croft et al., 2012), despite I_h being significantly upregulated.

We find that I_h induces a significant speeding of the membrane time-constant of RP3V kisspeptin neurons, an effect that is greater in proestrous mice. This effect may be due to tonic activity of the channels mediating I_h around −60 mV (the potential at which most of our experiments were performed) or to the fast, instantaneous component of I_h (Proenza et al., 2002). Regardless of the mechanism, this will have repercussions on the integration of subthreshold events such as synaptic currents, presumably speeding up synaptic potentials and limiting their temporal summation as in other neurons (Robinson and Siegelbaum, 2003; Biel et al., 2009).

Activation of I_h also results in a post-hyperpolarization rebound potential, which often triggers the firing of action potentials. In a few RP3V kisspeptin neurons, we observe that I_h-dependent rebound depolarization is responsible for most of the rebound firing. In most kisspeptin neurons, however, I_h has a modulatory role, and our data are consistent with a greater role of I_h in tuning the timing of rebound firing in proestrous RP3V kisspeptin neurons. Interestingly, a recent study of thalamic neurons reported a similar role of I_h in the timing of rebound firing (Ying et al., 2011).

It is important to note, however, that our examination of the potential consequences of I_h upregulation in RP3V kisspeptin neurons is limited by the fact that the electrical activity of these cells in brain slices may not be a faithful representation of the situation *in vivo*. For example, ongoing synaptic activity is much higher *in vivo* than in brain slices (Paré et al., 1998). Considering the role of I_h in synaptic integration (Robinson and Siegelbaum, 2003; Biel et al., 2009) and in the tuning of rebound firing, the upregulation of I_h in proestrous RP3V kisspeptin neurons may in fact have a significant impact on their spontaneous firing *in vivo*, despite our observation that it does not in slices.

In conclusion, we demonstrate that circulating E_2 drives substantial estrous cycle plasticity in the expression and function of I_h in RP3V kisspeptin neurons. This is the first evidence, to our knowledge, that I_h in central neurons is modulated by fluctuating gonadal steroid levels in the cycling female. The highest expression of I_h occurs on proestrus in RP3V kisspeptin neurons, and this may be involved in mediating the estrogen positive feedback signal to GnRH neurons. While several ion channels have been shown to be regulated by E_2 in gonadectomized animal models (Christian and Moenter, 2010; Rønnekleiv et al., 2012), the present study provides a rare example of a membrane current that, in addition, exhibits estrous cycle plasticity in intact female animals.

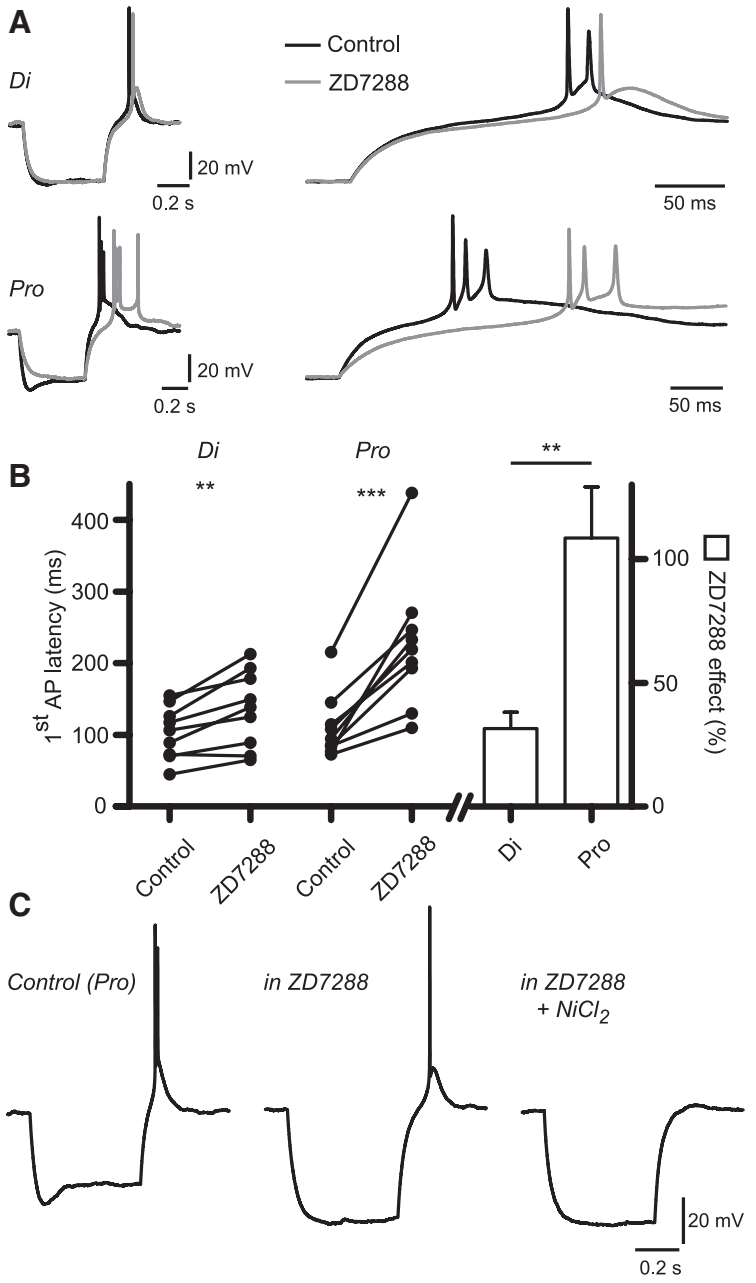

Figure 8. I_h differentially alters the timing of rebound firing in diestrous and proestrous RP3V kisspeptin neurons. ***A***, Example traces of the rebound firing following injection of a hyperpolarizing current in a diestrous and a proestrous RP3V kisspeptin neuron, in the absence (black) and in the presence (gray) of 10 μM ZD7288 (left). Current injection was adjusted in the proestrous neuron to reach a similar steady-state hyperpolarization (control: −80 pA; ZD7288: −40 pA). Higher-resolution traces (right) show that the ZD7288-induced delay of AP firing is longer in proestrous than in diestrous RP3V kisspeptin neurons. ***B***, Graph summarizing the effect of ZD7288 on rebound firing latency in diestrus ($n = 9$ neurons, 4 mice) and in proestrus ($n = 9$ neurons, 5 mice). $^{**}p < 0.01$, $^{***}p < 0.001$. ***C***, Example traces of a proestrous RP3V kisspeptin neuron in which rebound firing is not prevented by ZD7288 but is abolished by 200 μM $NiCl_2$. Similar results were obtained in six neurons from three mice in total.

References

Adachi S, Yamada S, Takatsu Y, Matsui H, Kinoshita M, Takase K, Sugiura H, Ohtaki T, Matsumoto H, Uenoyama Y, Tsukamura H, Inoue K, Maeda K (2007) Involvement of anteroventral periventricular metastin/kisspeptin neurons in estrogen positive feedback action on luteinizing hormone release in female rats. J Reprod Dev 53:367–378. CrossRef Medline

Bi R, Foy MR, Vouimba RM, Thompson RF, Baudry M (2001) Cyclic changes in estradiol regulate synaptic plasticity through the MAP kinase pathway. Proc Natl Acad Sci U S A 98:13391–13395. CrossRef Medline

Biel M, Wahl-Schott C, Michalakis S, Zong X (2009) Hyperpolarization-activated cation channels: from genes to function. Physiol Rev 89:847–885. CrossRef Medline

Brinton RD (2009) Estrogen-induced plasticity from cells to circuits: predictions for cognitive function. Trends Pharmacol Sci 30:212–222. CrossRef Medline

Bronson FH (1981) The regulation of luteinizing hormone secretion by estrogen: relationships among negative feedback, surge potential, and male stimulation in juvenile, peripubertal, and adult female mice. Endocrinology 108:506–516. CrossRef Medline

Bronson FH, Vom Saal FS (1979) Control of the preovulatory release of luteinizing hormone by steroids in the mouse. Endocrinology 104:1247–1255. CrossRef Medline

Caligioni CS (2009) Assessing reproductive status/stages in mice. Curr Protoc Neurosci Appendix 4:Appendix 4I. CrossRef Medline

Christian CA, Moenter SM (2010) The neurobiology of preovulatory and estradiol-induced gonadotropin-releasing hormone surges. Endocr Rev 31:544–577. CrossRef Medline

Chu Z, Takagi H, Moenter SM (2010) Hyperpolarization-activated currents in gonadotropin-releasing hormone (GnRH) neurons contribute to intrinsic excitability and are regulated by gonadal steroid feedback. J Neurosci 30:13373–13383. CrossRef Medline

Clarkson J, Herbison AE (2009) Oestrogen, kisspeptin, GPR54 and the pre-ovulatory luteinising hormone surge. J Neuroendocrinol 21:305–311. CrossRef Medline

Clarkson J, d'Anglemont de Tassigny X, Moreno AS, Colledge WH, Herbison AE (2008) Kisspeptin-GPR54 signaling is essential for preovulatory gonadotropin-releasing hormone neuron activation and the luteinizing hormone surge. J Neurosci 28:8691–8697. CrossRef Medline

de Croft S, Piet R, Mayer C, Mai O, Boehm U, Herbison AE (2012) Spontaneous kisspeptin neuron firing in the adult mouse reveals marked sex and brain region differences but no support for a direct role in negative feedback. Endocrinology 153:5384–5393. CrossRef Medline

DiFrancesco D, Tortora P (1991) Direct activation of cardiac pacemaker channels by intracellular cyclic AMP. Nature 351:145–147. CrossRef Medline

Ducret E, Gaidamaka G, Herbison AE (2010) Electrical and morphological characteristics of anteroventral periventricular nucleus kisspeptin and other neurons in the female mouse. Endocrinology 151:2223–2232. CrossRef Medline

Foy MR, Baudry M, Akopian GK, Thompson RF (2010) Regulation of hippocampal synaptic plasticity by estrogen and progesterone. Vitam Horm 82:219–239. CrossRef Medline

Frazão R, Cravo RM, Donato J Jr, Ratra DV, Clegg DJ, Elmquist JK, Zigman JM, Williams KW, Elias CF (2013) Shift in Kiss1 cell activity requires estrogen receptor α. J Neurosci 33:2807–2820. CrossRef Medline

Glidewell-Kenney C, Hurley LA, Pfaff L, Weiss J, Levine JE, Jameson JL (2007) Nonclassical estrogen receptor alpha signaling mediates negative feedback in the female mouse reproductive axis. Proc Natl Acad Sci U S A 104:8173–8177. CrossRef Medline

Good M, Day M, Muir JL (1999) Cyclical changes in endogenous levels of

oestrogen modulate the induction of LTD and LTP in the hippocampal CA1 region. Eur J Neurosci 11:4476–4480. CrossRef Medline

Gottsch ML, Popa SM, Lawhorn JK, Qiu J, Tonsfeldt KJ, Bosch MA, Kelly MJ, Rønnekleiv OK, Sanz E, McKnight GS, Clifton DK, Palmiter RD, Steiner RA (2011) Molecular properties of Kiss1 neurons in the arcuate nucleus of the mouse. Endocrinology 152:4298–4309. CrossRef Medline

Harris NC, Constanti A (1995) Mechanism of block by ZD 7288 of the hyperpolarization-activated inward rectifying current in guinea pig substantia nigra neurons in vitro. J Neurophysiol 74:2366–2378. Medline

Herbison AE (2006) Physiology of the gonadotropin-releasing hormone neuronal network. In: Knobil and Neill's physiology of reproduction, Ed 3, pp 1415–1482,VII. Amsterdam: Elsevier.

Herbison AE (2008) Estrogen positive feedback to gonadotropin-releasing hormone (GnRH) neurons in the rodent: the case for the rostral periventricular area of the third ventricle (RP3V). Brain Res Rev 57:277–287. CrossRef Medline

Lewis AS, Schwartz E, Chan CS, Noam Y, Shin M, Wadman WJ, Surmeier DJ, Baram TZ, Macdonald RL, Chetkovich DM (2009) Alternatively spliced isoforms of TRIP8b differentially control h channel trafficking and function. J Neurosci 29:6250–6265. CrossRef Medline

Liu X, Porteous R, d'Anglemont de Tassigny X, Colledge WH, Millar R, Petersen SL, Herbison AE (2011) Frequency-dependent recruitment of fast amino acid and slow neuropeptide neurotransmitter release controls gonadotropin-releasing hormone neuron excitability. J Neurosci 31:2421–2430. CrossRef Medline

Luine VN, Frankfurt M (2012) Estrogens facilitate memory processing through membrane mediated mechanisms and alterations in spine density. Front Neuroendocrinol 33:388–402. CrossRef Medline

Mayer C, Acosta-Martinez M, Dubois SL, Wolfe A, Radovick S, Boehm U, Levine JE (2010) Timing and completion of puberty in female mice depend on estrogen receptor alpha-signaling in kisspeptin neurons. Proc Natl Acad Sci U S A 107:22693–22698. CrossRef Medline

McCormick DA, Bal T (1997) Sleep and arousal: thalamocortical mechanisms. Annu Rev Neurosci 20:185–215. CrossRef Medline

McEwen BS, Akama KT, Spencer-Segal JL, Milner TA, Waters EM (2012) Estrogen effects on the brain: actions beyond the hypothalamus via novel mechanisms. Behav Neurosci 126:4–16. CrossRef Medline

Oakley AE, Clifton DK, Steiner RA (2009) Kisspeptin signaling in the brain. Endocr Rev 30:713–743. CrossRef Medline

Pape HC (1996) Queer current and pacemaker: the hyperpolarization-activated cation current in neurons. Annu Rev Physiol 58:299–327. CrossRef Medline

Paré D, Shink E, Gaudreau H, Destexhe A, Lang EJ (1998) Impact of spontaneous synaptic activity on the resting properties of cat neocortical pyramidal neurons In vivo. J Neurophysiol 79:1450–1460. Medline

Pian P, Bucchi A, Robinson RB, Siegelbaum SA (2006) Regulation of gating and rundown of HCN hyperpolarization-activated channels by exogenous and endogenous PIP2. J Gen Physiol 128:593–604. CrossRef Medline

Piskorowski R, Santoro B, Siegelbaum SA (2011) TRIP8b splice forms act in concert to regulate the localization and expression of HCN1 channels in CA1 pyramidal neurons. Neuron 70:495–509. CrossRef Medline

Proenza C, Tran N, Angoli D, Zahynacz K, Balcar P, Accili EA (2002) Different roles for the cyclic nucleotide binding domain and amino terminus in assembly and expression of hyperpolarization-activated, cyclic nucleotide-gated channels. J Biol Chem 277:29634–29642. CrossRef Medline

Qiu J, Fang Y, Bosch MA, Rønnekleiv OK, Kelly MJ (2011) Guinea pig kisspeptin neurons are depolarized by leptin via activation of TRPC channels. Endocrinology 152:1503–1514. CrossRef Medline

Robinson RB, Siegelbaum SA (2003) Hyperpolarization-activated cation currents: from molecules to physiological function. Annu Rev Physiol 65:453–480. CrossRef Medline

Rønnekleiv OK, Bosch MA, Zhang C (2012) 17beta-oestradiol regulation of gonadotrophin-releasing hormone neuronal excitability. J Neuroendocrinol 24:122–130. CrossRef Medline

Santoro B, Liu DT, Yao H, Bartsch D, Kandel ER, Siegelbaum SA, Tibbs GR (1998) Identification of a gene encoding a hyperpolarization-activated pacemaker channel of brain. Cell 93:717–729. CrossRef Medline

Santoro B, Wainger BJ, Siegelbaum SA (2004) Regulation of HCN channel surface expression by a novel C-terminal protein-protein interaction. J Neurosci 24:10750–10762. CrossRef Medline

Scharfman HE, Mercurio TC, Goodman JH, Wilson MA, MacLusky NJ (2003) Hippocampal excitability increases during the estrous cycle in the rat: a potential role for brain-derived neurotrophic factor. J Neurosci 23:11641–11652. Medline

Smith JT, Cunningham MJ, Rissman EF, Clifton DK, Steiner RA (2005) Regulation of Kiss1 gene expression in the brain of the female mouse. Endocrinology 146:3686–3692. CrossRef Medline

Smith JT, Popa SM, Clifton DK, Hoffman GE, Steiner RA (2006) Kiss1 neurons in the forebrain as central processors for generating the preovulatory luteinizing hormone surge. J Neurosci 26:6687–6694. CrossRef Medline

Srivastava DP (2012) Two-step wiring plasticity–a mechanism for estrogen-induced rewiring of cortical circuits. J Steroid Biochem Mol Biol 131:17–23. CrossRef Medline

Warren SG, Humphreys AG, Juraska JM, Greenough WT (1995) LTP varies across the estrous cycle: enhanced synaptic plasticity in proestrus rats. Brain Res 703:26–30. CrossRef Medline

Wintermantel TM, Campbell RE, Porteous R, Bock D, Gröne HJ, Todman MG, Korach KS, Greiner E, Pérez CA, Schütz G, Herbison AE (2006) Definition of estrogen receptor pathway critical for estrogen positive feedback to gonadotropin-releasing hormone neurons and fertility. Neuron 52:271–280. CrossRef Medline

Woolley CS, McEwen BS (1992) Estradiol mediates fluctuation in hippocampal synapse density during the estrous cycle in the adult rat. J Neurosci 12:2549–2554. Medline

Ying SW, Tibbs GR, Picollo A, Abbas SY, Sanford RL, Accardi A, Hofmann F, Ludwig A, Goldstein PA (2011) PIP2-mediated HCN3 channel gating is crucial for rhythmic burst firing in thalamic intergeniculate leaflet neurons. J Neurosci 31:10412–10423. CrossRef Medline

Zolles G, Klöcker N, Wenzel D, Weisser-Thomas J, Fleischmann BK, Roeper J, Fakler B (2006) Pacemaking by HCN channels requires interaction with phosphoinositides. Neuron 52:1027–1036. CrossRef Medline